Check for updates

ADVANCED MATERIALS
www.advmat.de

Boosting Contact Electrification by Amorphous Polyvinyl Alcohol Endowing Improved Contact Adhesion and Electrochemical Capacitance

*Lisa Serairi, Chiara Santillo, Philippe Basset, Marino Lavorgna, and Giuseppina Pace**

Ion conductive hydrogels are relevant components in wearable, biocompatible, and biodegradable electronics. Polyvinyl-alcohol (PVA) homopolymer is often the favored choice for integration into supercapacitors and energy harvesters as in sustainable triboelectric nanogenerators (TENGs). However, to further improve hydrogel-based TENGs, a deeper understanding of the impact of their composition and structure on devices performance is necessary. Here, it is shown how ionic hydrogels based on an amorphous-PVA (a-PVA) allow to fabricate TENGs that outperform the one based on the homopolymer. When used as tribomaterial, the Li-doped a-PVA allows to achieve a twofold higher pressure sensitivity compared to PVA, and to develop a conformable e-skin. When used as an ionic conductor encased in an elastomeric tribomaterial, 100 mW cm^{-2} average power is obtained, providing 25% power increase compared to PVA. At the origin of such enhancement is the increased softness, stronger adhesive contact, higher ionic mobility (> 3,5-fold increase), and long-term stability achieved with Li-doped a-PVA. These improvements are attributed to the high density of hydroxyl groups and amorphous structure present in the a-PVA, enabling a strong binding to water molecules. This work discloses novel insights on those parameters allowing to develop easy-processable, stable, and highly conductive hydrogels for integration in conformable, soft, and biocompatible TENGs.

1. Introduction

The development of novel wearable, flexible, and conformable devices, as found in health monitoring systems, has increased the search for alternative sustainable energy sources different from batteries. To reach this goal, recent efforts are mostly directed to promote a transition toward biodegradable, biocompatible, and self-powered devices. Among mechanical energy harvesters, triboelectric nanogenerators (TENGs) can foster this transition as they can efficiently convert the widely distributed and dispersed environmental mechanical energy into a sustainable electrical power source.[1–3] Since 2012, TENGs have received widespread attention as power sources to be integrated into low power IoT,[4] wearables,[5] and conformable electronics, such as the e-skin.[6] Various approaches have been explored to boost TENGs power density, including device configuration design,[7] tailoring of the triboelectric material (tribomaterial) chemical composition,[8,9] electrode and interlayer engineering,[10–12] and through the increase of tribomaterials surface density, dielectric constant,[13,14] ionic conductivity,[15,16] and of the electrode capacitance.[17,18]

More recently, the presence of strong adhesion forces established between the electropositive and electronegative tribomaterials,[19] and their mechanical softness,[20] has been highlighted as also contributing to a large increase in TENGs power output. Kim et al. showed how TENGs power correlates with the Young's modulus of polydimethylsiloxane (PDMS) used as tribomaterial.[21] A detailed study demonstrating the effect of mechanical properties of strongly adhesive tribomaterials (as sticky tape) on the electrical output of TENGs, was presented by Zhang et al.[22,23]

L. Serairi, P. Basset
Univ Gustave Eiffel
CNRS
ESYCOM
Marne-la-Vallée F-77454, France

C. Santillo, M. Lavorgna
Institute for Polymers
Composites and Biomaterials
National Research Council of Italy
P.le E. Fermi 1, Portici 80055, Italy

M. Lavorgna
Institute for Polymers
Composites and Biomaterials
National Research Council of Italy
Via Previati, 1/E, Lecco 23900, Italy

G. Pace
Institute for Microelectronics and Microsystems
National Research Council (IMM-CNR)
Via C. Olivetti 2, Agrate 20864, Italy
E-mail: giuseppina.pace@cnr.it

The ORCID identification number(s) for the author(s) of this article can be found under https://doi.org/10.1002/adma.202403366

© 2024 The Author(s). Advanced Materials published by Wiley-VCH GmbH. This is an open access article under the terms of the Creative Commons Attribution License, which permits use, distribution and reproduction in any medium, provided the original work is properly cited.

DOI: 10.1002/adma.202403366

The authors demonstrated that the fast detachment between a triboelectric adhesive tape and a solid-state electrode, was responsible for an increased energy dissipation area, that favored an improved peeling triboelectrification. From the tribomaterial chemical design point of view, more adhesive contacts are typically found between surfaces which can interact by mean of weak bonding, such as hydrogen bonds and van der Waals interactions.[24,25] However, specific strategies on how to increase contact electrification through improved tribomaterials adhesion properties, have not been sufficiently explored so far.

Additionally, for applications such as implantable biomedical sensors and human–machine interfaces, polymer hydrogels are growing as valuable components,[26,27] due to their easy processing, scalable, and reproducible synthesis, biocompatibility, stretchability, and transparency.[28,29]

In TENGs, hydrogels are employed either as active tribomaterials, or as ionic conductors encapsulated in an elastomeric scaffold. It is shown that when film made from hydrogels are used as active tribomaterial, their triboelectrification efficiency increases upon ionic doping.[16,30–33]

Ionic conductive hydrogels encased into an impermeable tribomaterial scaffold as Ecoflex,[34–36] silicone (Si)-rubber,[37] or even scotch tape,[38,39] allow to fabricate transparent and flexible TENGs with improved time-stability.[40,41] In this device configuration, the hydrogel's ions migration toward the electrode is triggered by the contact electrification occurring at the elastomer external surface, and is responsible for the increased electrical double layer capacitance (EDLC) of the TENG's electrodes.[38,39,42]

Hydrogels based on polyvinyl alcohol (PVA) are the most investigated in biocompatible and biodegradable electronics applications.[43–47] A fully dissolvable TENG based on PVA used as active tribomaterial has been demonstrated by Liang et al.[48] High electrical output, reaching an open circuit voltage of few hundreds volts (up to 400 V and ≈10 µA),[49] is found in TENGs comprising an ionic and electrically conducting electrode composed of a MXene-PVA composite hydrogel encased in an Ecoflex scaffold.[50] However, due to its regular chemical structure, the PVA homopolymer favors the formation of crystalline domains both in concentrated aqueous solution and in the bulk state, which reduces solution processability, film transparency and shelf-life stability.[51,52] Since hydrogels are water swollen 3D polymers networks, their properties are strongly dependent on the capability to retain water over long periods of time and under different ambient conditions.[53]

Here, we show how to improve the electrical performance of hydrogel-based TENGs, by employing a PVA derivative endowing a higher hydration degree compared to the more common PVA homopolymer. Specifically, we employed a highly amorphous PVA derivative (also referred in the literature as HAVOH, hereafter as a-PVA), consisting of a polyvinyl alcohol chain modified with butene-diol-type monomers. Compared to the parent PVA homopolymer, the introduction of ramified and hydroxylated monomers is known to contribute to contrast the crystallization process, to infer to the amorphous phase a higher resistance to the macromolecular chains' relaxations[54] and to provide an excellent water solubility.[55] We show that a high hydration and a strong binding to water molecules are important factors to improve hydrogel-based TENGs performance due to the increased i) material softness, ii) contact adhesion and thus triboelectrification charge density, and iii) hydrogel ionic conductivity. The ions conductive hydrogels obtained by mixing the PVA (or a-PVA) with Li salts (PVA:Li and a-PVA:Li, respectively), present a large difference in water content. Specifically, strongly bound water, i.e., water that is lost above the pure water boiling temperature of 100 °C, is found to be 5.4% in PVA:Li and 12.5% in a-PVA:Li (lost at 150 °C). The higher water uptake of the 3D-polymer network, allows for an easier solution processing of the a-PVA formulations, increased adhesion of the obtained film, higher ionic mobility (7.4×10^{-4} S cm^{-1} for a-PVA:Li and 2.0×10^{-4} S cm^{-1} for PVA:Li, 50:50 w/w) and longtime stability (more than 1 year).

We demonstrate the favorable impact of the above properties on TENGs electrical output in two device's configurations where the hydrogel formulations have been employed to prepare either the tribomaterial or the ionic conductor. In the first configuration, the hydrogel-based film is used as a friction tribomaterial. Here, the a-PVA allowed to achieve more than a twofold increase in both the average power and pressure sensitivity with respect to the PVA homopolymer (2.1 V kPa^{-1} for a-PVA:Li and 0.9 V kPa^{-1} for PVA:Li; @5 Hz), with a linearity range that extends from 2 kPa up to 14 kPa. To the best of our knowledge, this sensitivity is the highest reported so far for TENGs sensors based on single layer, nonfluorinated, and/or nonpatterned tribomaterials.[56,57] In fact, a common strategy used to raise pressure sensitivity is to increase the tribomaterial surface area, e.g., using fiber like structures or nano/micropatterning. A record value of ≈15 V kPa^{-1} was reported by Xu et al.,[58] for tribomaterial based on porous PDMS, while a sensitivity of ≈9.5 V kPa^{-1} was reported by Lia et al.,[59] who showed a TENG sensor comprising an Ecoflex surface patterned with a triangular microprism microstructure. However, the reported linearity range was limited to 0–5 kPa. Here, a high sensitivity and large linearity range is achieved with no need of surface nano/microstructuring, but rather using a flat surface (rms roughness < 4 nm), thus reducing the required devices fabrication steps and costs, and overcoming the mechanical instability of the patterned structure after continuous contact/separation events, that largely limits the sensor lifetime. We demonstrate that the improved contact electrification endowed by a-PVA:Li compared to the PVA:Li films, is due to the increased adhesive and conformal contact that is established between the two friction layers during TENGs operation.[19–21] To show their effective sensing capabilities, single electrode TENGs based on a-PVA:Li conductive hydrogels, have also been tested as conformable tactile sensors in an e-skin prototype. These a-PVA hydrogel based TENGs show an increased flexibility and shelf-life stability over at least 1 year.

To further demonstrate the impact of the water entrapped in the polymer network, we also fabricated TENGs where the a-PVA conductive hydrogel is integrated as an ionic conductor into an elastomeric silicone (Si)-rubber scaffold. Due to its higher ionic mobility (≈fourfold increase), the a-PVA:Li conductive hydrogels allow to achieve an instant peak power density of 840 mW m^{-2} (average power 102 mW m^{-2}; V_{OC} 350 V, @ 5 Hz, 15 N), corresponding to a 25% increase compared to TENGs based on Li-doped PVA hydrogels, and to almost a 40%

© 2024 The Author(s). Advanced Materials published by Wiley-VCH GmbH

15214095, 2024, 27, Downloaded from https://advanced.onlinelibrary.wiley.com/doi/10.1002/adma.202403366 by Yonsei University Library, Wiley Online Library on [21/08/2025]. See the Terms and Conditions (https://onlinelibrary.wiley.com/terms-and-conditions) on Wiley Online Library for rules of use; OA articles are governed by the applicable Creative Commons License

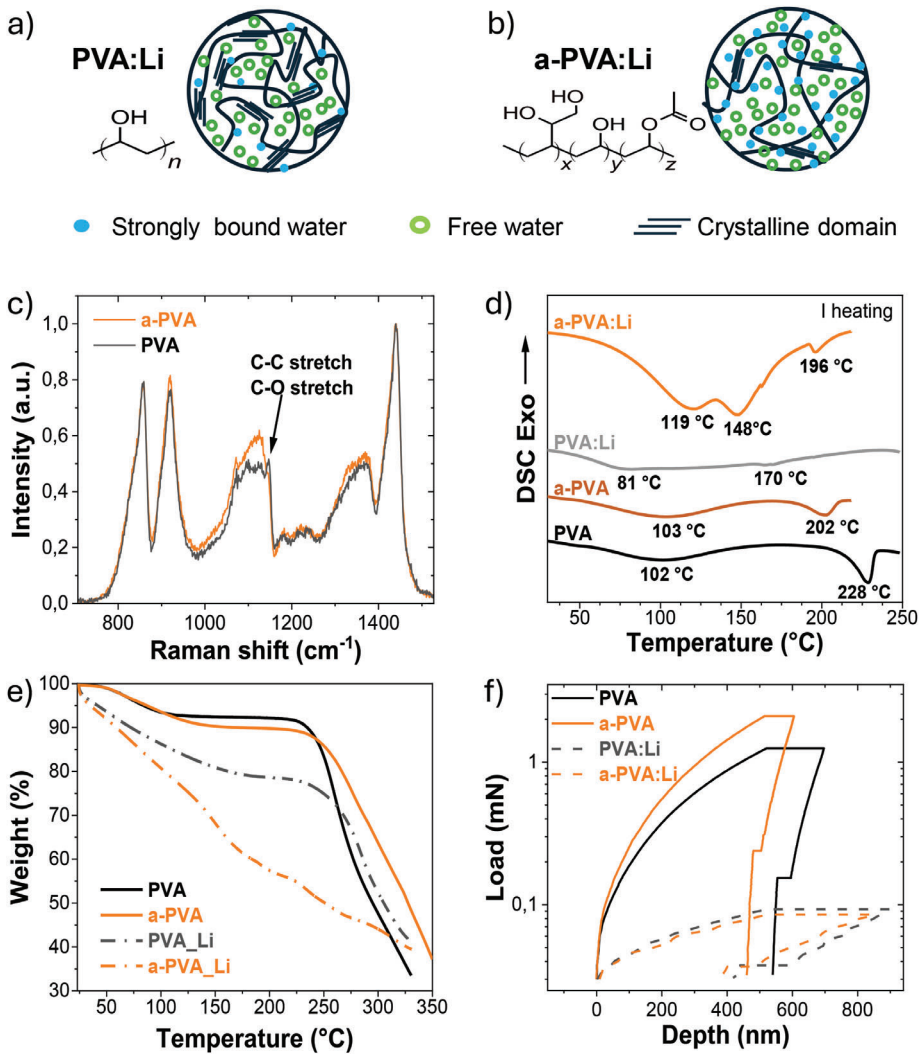

Figure 1. Chemical structure of the investigated polymers and scheme of the different water uptake and hydrogel crystallinity present in the ion conductive homopolymer PVA:Li a) and in the amorphous copolymer a-PVA:Li b). In the schemes, the electrolytes ions have been omitted for simplicity. c) Normalized Raman spectra acquired on PVA and a-PVA films. d) DSC and e) TGA recorded on PVA and a-PVA films. f) Nanoindentation measurements acquired on aged samples (≈1 year from film preparation).

increase with respect to the one made of Si-rubber only. Such high electrical output sets among, and surpass, even the best performance reached in hydrogel based TENGs operating in single electrode mode and integrating mixed ionic and electronic conductors, where conductive additives such as MXenes[49,50] or metallic compounds[35,38] are dispersed in the hydrogel. Our devices also show long cycling (more than 5000 continuous cycles) and shelf-life stability in ambient conditions (more than 3 months).

Therefore, in both device configurations, the stronger binding to water molecules and the higher water uptake achieved by the a-PVA:Li with respect to the PVA counterpart, are the main factors responsible for the improvement of those physical-chemical parameters, such as softness, flexibility, surface adhesion, and ionic conductivity, all leading to enhanced TENGs electrical performance and time stability. The achievement of high-pressure sensitivity with a simple device configuration, as the one reported here, is essential for the easy fabrication and development of conformable e-skin and touch sensors. Overall, this study provides novel insights on the chemical design of polymer hydrogels owing improved ionic conductivity and surface triboelectrification efficiency, thus contributing to the development of high performing biocompatible TENGs.

2. Results and Discussion

2.1. Chemical and Structural Characterization of Hydrogel Films

Although it is reported that high molecular weight PVA (> 140 000 g mol^{-1}) can dissolve at ≈80 °C, this homopolymer shall be heated up to 135–140 °C [60] to reach the complete dissolution of the polymer aggregates still present in solution,[52] especially at high concentration (≈100 g L^{-1}). In addition, for low

© 2024 The Author(s). Advanced Materials published by Wiley-VCH GmbH

15214095, 2024, 27, Downloaded from https://advanced.onlinelibrary.wiley.com/doi/10.1002/adma.202403366 by Yonsei University Library, Wiley Online Library on [21/08/2025]. See the Terms and Conditions (https://onlinelibrary.wiley.com/terms-and-conditions) on Wiley Online Library for rules of use; OA articles are governed by the applicable Creative Commons License

temperatures (80–90 °C) incomplete dissolution easily occurs and polymer particles precipitate during the drying step of the hydrogel film,[28] deteriorating the ionic mobility and film uniformity. Besides, the time dependent polymer recrystallization process increases the mechanical fragility of the resulting PVA films upon aging.

The amorphous PVA derivative (a-PVA) investigated in this work, containing diol type (1-butene-3,4-diole) and acetate monomers distributed along the polymer backbone (**Figure 1**a,b), does not form extended crystalline domains, promoting a facile dissolution at low temperature (< 100 °C).[61] Thanks to the a-PVA copolymer chemical composition, clear, time stable and high concentrated solutions (100 g L^{-1}) could be obtained at temperature ≤100 °C. Furthermore, no particles precipitation occurred during film drying in ambient conditions.

The higher degree of crystallinity characterizing the PVA films compared to the a-PVA is shown in the Raman spectra reported in Figure 1c. Here, the presence of crystalline regions is highlighted by the C—C-stretching mode peak found at 1148 cm^{-1} (Figure 1c).[62–64] The complete peak assignment of the Raman modes is reported in Figure S1 (Supporting Information). Water retention measurements show that steady state equilibrium in ambient condition is reached by both polymer films after overnight drying in air (in Figure S4, Supporting Information). Differential scanning calorimetry (DSC) performed on the hydrogel films (Figure 1d) in the range from 70 °C to about 250 °C, shows a melting temperature of 202 °C for the a-PVA film, which is 26 °C lower than in PVA. This confirms that the a-PVA films exhibit a reduced degree of ordered crystalline domains compared to the PVA (23% and 46%, respectively).

We selected LiCl as the electrolyte for the optimization of the conductive hydrogels, due to its high solubility in water solutions, and to the Li^+ higher mobility than other alkaline metal cations.[65] When used as active tribomaterial in TENGs, the optimal conductive hydrogel formulation is found for a polymer-to-LiCl weight ratio of 100:20 w/w. This ratio represents the best trade-off between polymer solubility and good film-forming capabilities. The addition of LiCl inhibits the crystallization in both the PVA and a-PVA based films (Raman spectra in the Supporting Information) as expected, due to its high hygroscopicity and the establishment of polymer-ions interactions disrupting the inter and intramolecular bonds. Compared to the pristine films, DSC data acquired on a-PVA:Li and PVA:Li films (Figure 1d), show an increased number of endothermic thermal features (II heating step of DSC, in the Supporting Information). Such features can be ascribed to the presence of different binding configurations of the water molecules, which can interact with the polymer chain and the Li^+ and Cl^- ions, through H-bonding or solvating interactions. However, this is more evident in the a-PVA:Li case, where more endothermic thermal features than in PVA:Li are detected, highlighting the presence of multiple types of polymer-water-ions interactions. The peaks observed at 119 and 148 °C demonstrate that in a-PVA:Li the water molecules can strongly interact with the polymer chains and the electrolyte ions in the systems. Opposite to PVA:Li, in a-PVA:Li films most of these water species can be removed only at temperatures significantly higher than those characteristics of free and bound water in polymeric substrates,[66] leading to the higher water uptake observed in a-PVA:Li.

Table 1. Fraction of the total water content and of each type of water species present in each film.

	Total water content lost @180 °C [%]	Free water lost @100 °C [%]	Strongly bound water lost @150 °C [%]
PVA	7.7	6.5	1.0
a-PVA	10.1	6.5	3.2
PVA:Li	20.8	14	5.4
a-PVA:Li	39.4	20	12.5

In agreement with DSC data, thermal gravimetric analysis (TGA, Figure 1e) shows that the a-PVA:Li sample is characterized by several weight losses ascribed to a large variety of water-coordinated species. The total water fraction present in each film (**Table 1**) was found to be almost a factor 2 higher in the a-PVA:Li formulation compared to the PVA:Li (39.4% and 20.8%, respectively, more details on data analysis can be found in the Supporting Information). Similarly, around 14 and 20 wt% of such water is found to be present as free-water (lost at 100 °C), and around 5.4 and 12.5 wt% is present as strongly interacting water (lost at 150 °C) in PVA:Li and a-PVA:Li, respectively.

The above spectroscopic and thermal analysis confirm both the greater extent of the amorphous structure and the higher capability to retain strongly interacting water molecules achieved by the a-PVA and a-PVA:Li with respect to the homopolymer analogues. These features are also reflected in the hydrogel films mechanical properties investigated by means of nanoindentation experiments.

Differently from standard tensile measurements, nanoindentation allow to access the surface mechanical properties of the different hydrogel films investigated in this work, while keeping the same sample configuration used to fabricate the TENGs reported in Figure 3 (thin film coatings on solid substrates). Figure 1f shows the mechanical response of the two polymers films (PVA and a-PVA) with or without Li salt, acquired on samples that have been stored for almost 1 year in ambient conditions. Although PVA is more crystalline than a-PVA, the maximum load to be applied to reach the expected tip penetration is comparable in both cases. This can be due to the strong intra and inter-chain interactions present in the amorphous phase of both polymers allowing to sustain high mechanical stress loads. Figure 1f also demonstrates how LiCl significantly reduces the mechanical hardness of both PVA and a-PVA. The hardness modulus decreases of more than one order of magnitude in presence of the Li salt in both films demonstrating the softer character of the Li-conductive hydrogels even after 1 year storage in ambient condition (0.13 GPa for PVA and 0.017 Gpa for PVA:Li; 0.26 GPa for a-PVA, and 0.018 GPa for a-PVA:Li). This is consistent with the presence of the highly hygroscopic Li-salt, responsible for a more water-swollen polymer matrix present in the conductive hydrogels with a macromolecular network differently crosslinked by H-bonding compared to the pristine polymers.

The high water content achieved by the a-PVA:Li hydrogel is also expected to increase its ionic conductivity. This is confirmed by impedance spectroscopy studies (in Figure S10, Supporting Information) performed on hydrogels-based films prepared from the 100:20 w/w formulations and measured after overnight

© 2024 The Author(s). Advanced Materials published by Wiley-VCH GmbH

15214095, 2024, 27, Downloaded from https://advanced.onlinelibrary.wiley.com/doi/10.1002/adma.202403366 by Yonsei University Library, Wiley Online Library on [21/08/2025]. See the Terms and Conditions (https://onlinelibrary.wiley.com/terms-and-conditions) on Wiley Online Library for rules of use; OA articles are governed by the applicable Creative Commons License

15214095, 2024, 27, Downloaded from https://advanced.onlinelibrary.wiley.com/doi/10.1002/adma.202403366 by Yonsei University Library, Wiley Online Library on [21/08/2025]. See the Terms and Conditions (https://onlinelibrary.wiley.com/terms-and-conditions) on Wiley Online Library for rules of use; OA articles are governed by the applicable Creative Commons License

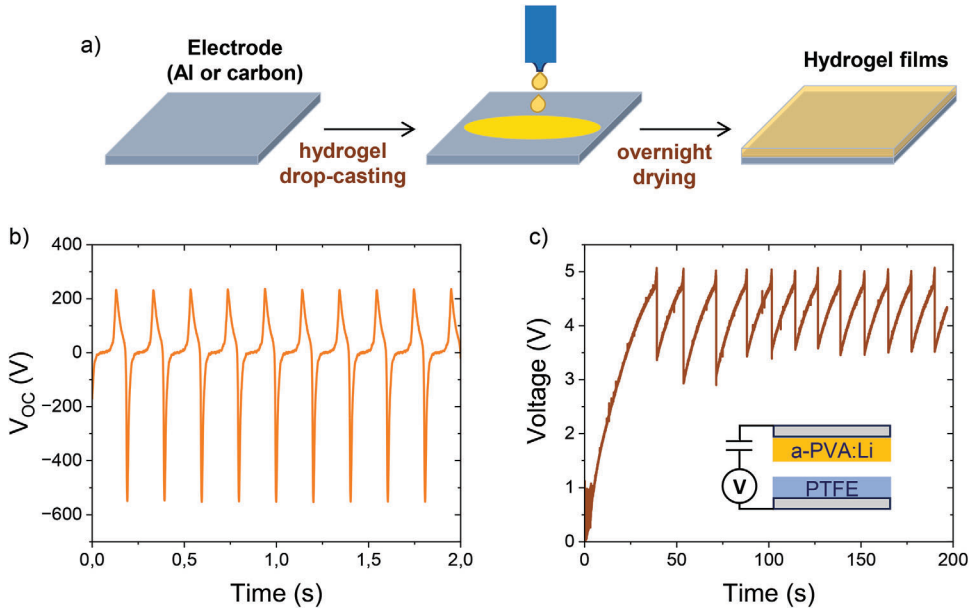

Figure 2. a) Schematic of the hydrogel-based film deposition on electrode. b) Open circuit voltage (V_{OC}) measured on a TENG operating in contact-separation mode (average power @5 Hz: 79.5 mW m^{-2}, force load 10 N, 5 mm maximum airgap). The electropositive tribomaterial is a polymer film based on a-PVA:Li (w/w, 100:20) and the electronegative tribomaterial is a pre-charged PTFE film. c) Continuous charge/discharge dynamic of a capacitor (1 µF, 5 V) by using a commercial LTC-3588 conditioning circuit. Inset figure c) scheme of the TENG device configuration under test.

drying. We found an ionic conductivity that is almost one order of magnitude higher in the a-PVA:Li compared to the PVA:Li films (1.6×10^{-4} and 2.5×10^{-5} S m^{-1}, respectively).

Overall, the ensemble of the morphological, thermal, and mechanical studies show that the added value of the novel a-PVA copolymer over the homopolymer is manifold: i) it fully dissolves even at high molecular weight (> 140 000 g mol^{-1}), high concentration (≈100 mg mL^{-1}), and low temperature (< 100 °C); ii) it exhibits a lower crystallinity hampering polymer chains ordered assembly and reorganization, reducing precipitation in solution, thus ensuring long time stability under storage in ambient conditions; iii) it sustains higher water uptake and stronger water-binding capability, due to the higher density of interacting hydroxyls sites and its amorphous morphology; therefore iv) it favors the good hydrogel wettability on solid substrates, higher ionic conductivity, improved film uniformity, and time stability. All these properties, synergistically determine the longer shelf-life stability, stronger adhesive contact upon friction, and improved flexibility of the a-PVA with respect to the homopolymer.

2.2. Role of Adhesive Forces on Contact Electrification

Typically, TENGs are designed to operate in one of the four working modes: a) contact-separation, b) lateral-sliding, c) single-electrode, and d) free-standing.[1] Surface triboelectrification occurs following the contact between two tribomaterials with a different electron affinity. In TENGs operating in contact-separation mode, due to the presence of the triboelectrification field established at the contact-step, an induction current is allowed to flow through the external circuit and a conversion of the negative mechanical work into electrical energy is obtained.

In TENGs, ion conductive hydrogels have been employed both to optimize the active tribomaterial or as electrolytic electrodes. When used as triboelectric layer, the presence of ions into the hydrogel formulation typically induces higher triboelectrification density compared to the pristine materials. When ion conductive hydrogels are integrated as ionic conductors, high ionic mobility and time stable hydration are the key factors to be targeted. In both application scenarios, the hydrogel water absorption is a fundamental parameter to be controlled for achieving improved softness, high ionic mobility, and good flexibility.

In this section, hydrogel films deposited on Al electrodes have been used as tribomaterial in TENGs operating in contact-separation mode (**Figures 2** and **3**). A first observation is that the adhesion on the Al electrode is strongly improved when using the a-PVA, while the PVA film peels-off from the substrate over time (inset Figure 3e,f). This improved adhesion is explained by the presence of the butene-diol monomers that increase the density of hydroxylated groups along the polymer chains and promote the amorphous structure of the polymer network, thus favoring the establishment of hydrogen bonding with the substrate as typical found in adhesive contacts. Fluorinated polymers (as polytetrafluoroethylene, PTFE or fluorinated ethylene propylene, FEP) are typically employed as electronegative tribomaterials in TENGs, as they easily negatively charge upon contact with different substrates. Here, a high power density (open circuit voltage, V_{OC} = 550 V; short circuit current, I_{SC} = 12 µA, average power 79.5 mW m^{-2}, @ 5 Hz, 10 N load; instant peak power 2 W m^{-2} in the Supporting Information) is achieved when a PTFE is precharged by mean of polyurethane glove rubbing, and it is used in combination whit the Li-doped a-PVA film (Figure 2b). In Figure 2c, a commercial conditioning circuit (LTC3588) was employed to rectify the TENG signal output and to provide a

© 2024 The Author(s). Advanced Materials published by Wiley-VCH GmbH

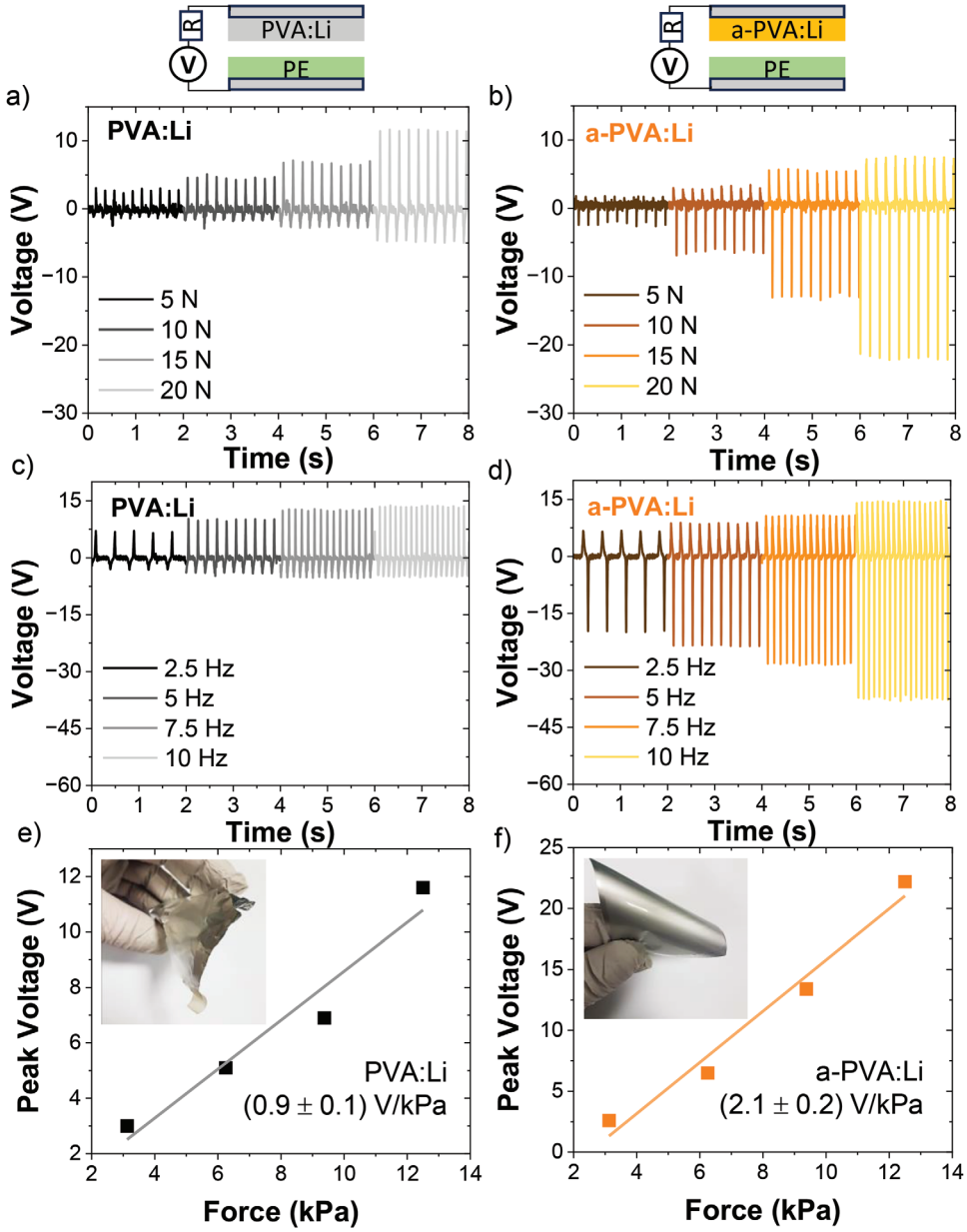

Figure 3. Top: scheme of TENGs device configuration. Voltage dependence on force load measured on TENGs integrating a) the PVA:Li or b) the a-PVA:Li films (100:20 w/w) used as active tribomaterials, and a PE film as reference (40 MΩ probe, area 4 × 4 cm^2, 5 mm spacing). Voltage dependence on frequency measured on TENGs based on c) PVA:Li and d) a-PVA:Li hydrogel films (force load 15 N). Force sensitivity extracted from voltage peak for e) PVA:Li and f) a-PVA:Li based TENGs. Insets in e) and f) show the optical image of aged PVA and a-PVA samples.

regulated electrical output suitable to charge a 1 μF capacitor. Figure 2c shows the continuous charge (up to 5 V) and discharge (down to ≈3–3.5 V) cycling, controlled by the conditioning circuit.

However, since triboelectrification charges can persist on the fluorinated polymer surface for months, especially in low humidity environment (< 40–50% humidity), and precharging is an easy artifact to occur, they cannot be used as a trustful reference material for comparative measurements.

Here, we selected polyester (PE) as reference tribomaterial since it can be easily discharged with an ionizing gun or with water wiping. Figure 3 shows the voltage output recorded from TENGs composed by a hydrogel film deposited on Al electrode on one side, and a PE film adhered on Al on the other side.

Pristine a-PVA and PVA films show similar performances (data in the Supporting Information). However, upon addition of LiCl the a-PVA:Li film outperform the PVA:Li, showing a 2-times higher average power (1.7 and 0.9 mW m^{-2} respectively, @ 5 Hz and 10 N; peak power in the Supporting Information).

The peak voltage polarity inversion, observed by comparing PVA:Li and a-PVA:Li based TENGs (Figure 3-a-b-c-d), is due to the opposite electrostatic charging undergone by the two

© 2024 The Author(s). Advanced Materials published by Wiley-VCH GmbH

15214095, 2024, 27, Downloaded from https://advanced.onlinelibrary.wiley.com/doi/10.1002/adma.202403366 by Yonsei University Library, Wiley Online Library on [21/08/2025]. See the Terms and Conditions (https://onlinelibrary.wiley.com/terms-and-conditions) on Wiley Online Library for rules of use; OA articles are governed by the applicable Creative Commons License

materials. Specifically, when coupled with the PE film, the PVA:Li hydrogel acts as positive tribomaterial, while the a-PVA:Li charges negatively, thus behaving as a negative tribomaterial. A similar polarity switch was also reported by Ryu et al., who have demonstrated that in tribomaterials based on ion conducting hydrogels, the proper selection of the electrolyte can switch the sign of the polarization of the triboelectrification charges.[16] In this work, the higher hydration, along with the more amorphous structure of the a-PVA:Li compared to the PVA:Li, can be responsible for a more efficient diffusion of the negative triboelectrification charges toward the Li^+ sites. This process would then lead to a more stable surface distribution of the negative triboelectric charge, thus reducing their reciprocal repulsion.

The force sensitivity (Figure 3e,f) was extracted from the voltage peak and was found to be 2-times higher in a-PVA:Li based TENGs than in PVA:Li (1.3 N V^{-1} or 2.1 V kPa^{-1} for a-PVA:Li; 0.5 V N^{-1} or 0.9 V kPa^{-1} for PVA:Li Li; @5 Hz, linearity range 2–14 kPa; active area 16 cm^2). The same electrical performance, as well as the polarity inversion, were observed both on freshly made and on 1 year aged devices, demonstrating the time stability and reproducibility of the measured electrical outputs.

The improved electrical output observed for the a-PVA:Li with respect to the PVA:Li, including the triboelectrification polarity inversion, shall be ascribed to the interplay of the morphological, mechanical, and electrochemical properties characterizing each type of hydrogel and that we address in the following discussion. To assess the role played by the surface morphology on the TENGs electrical performance, we acquired atomic force microscopy (AFM) and Scanning Electron Microscopy (SEM) images (reported in the Supporting Information). The pristine PVA and a-PVA films present similar surface morphology showing nanometer wide aggregates, which is also reflected in their similar TENGs output. A different surface morphology appears in the AFM images acquired on the PVA:Li and the a-PVA:Li films (100:20 w/w). However, due to their similar rms roughness (≈4 nm), this morphology difference cannot explain the large increase in the a-PVA:Li based TENGs electric output compared to PVA:Li. Therefore, other materials properties such as mechanical properties (material softness and adhesion forces) and ionic conductivity shall also be considered. The higher ionic mobility found for the a-PVA:Li (Section 2.1 and the Supporting Information), can foster an increase in the electrode capacitance due to a more efficient EDL formation (1.5 nF cm^{-2} for PVA:Li and 122 nF cm^{-2} for a-PVA:Li).[15]

In the previous section, we showed that the chemical composition and amorphous structure of the a-PVA:Li allows for an increased interaction with water molecules that are better entrapped within the polymer network. The increased softness observed for the Li-based films also enables a better conformal adhesion between the two tribomaterials during contact events, thus promoting an efficient triboelectric charge transfer.

An additional important consequence of the higher water content found in the a-PVA:Li, is the establishment of a soft and sticky adhesion occurring upon contact with the reference tribomaterial (Video in the Supporting Information). A more adhesive contact was previously identified as responsible for an increase in the energy dissipation area occurring during the detachment of two adhesive interfaces and leading to a higher yield of triboelectrification charge density.[19]

To directly correlate the rheological and tribological properties of each hydrogel-based film with the electrical response of their respective TENGs, we measured in situ (on-device) force–distance curves that are reported in **Figure** 4c. Since adhesion is strictly dependent on the chemical, mechanical, and morphological nature of the two materials placed into contact, the in situ measurements reflect the specific adhesive and mechanical behaviors expressed by each investigated pair of tribomaterials integrated into the operating TENGs. Therefore, the mechanical properties extrapolated from the in situ force–distance curves can be directly correlated with the electromechanical performance of the investigated TENG. Stronger adhesive forces are established between the a-PVA:Li film and the PE film with respect to the PVA:Li, showing more than a 3-times higher adhesion force and adhesion work (1.2 N and 1.0 μJ; 3.5 N and 3.8 μJ for PVA:Li and a-PVA:Li, respectively). Table S5 reported in the Supporting Information summarizes the adhesion force and adhesion work extracted from the in situ measurements.

Additional AFM force–distance curves acquired on the investigated film coatings, and reported in the Supporting Information,[67–69] further confirm that the a-PVA:Li undergoes a larger plastic deformation than PVA:Li and which is correlated to a higher dissipation energy, a lower stiffness, and a higher work of adhesion (49 N m^{-1} and 20 pJ in a-PVA:Li; 74 N m^{-1} and 13 pJ in PVA:Li, Table S6, Supporting Information).[68]

The adhesive contact strongly affects the charge and discharge dynamics of the TENG's electrodes and the devices time response (Figure 4a). Figure 4a-i shows the time dependent charge and discharge recorded over a single contact-and-separation cycle for TENGs operating in contact separation mode. The reference tribomaterial is a PE film adhered on Al substrate, while the investigated tribomaterials are, respectively, the PVA:Li, a-PVA:Li, and bare Al. The corresponding normalized voltage curves are reported in Figure 4a-ii. The charge and voltage dynamics clearly show the difference between the adhesive contact established at the interface between the PE and the a-PVA:Li film, and the nonsticky contact established with the PVA:Li and the bare Al. It is important to notice that the devices under study were measured more than 8 months after their fabrication, highlighting the time-stability of the adhesive contact. The a-PVA:Li showed the faster response time (5 ms) compared to the PVA:Li and Al based TENGs (18 and -16 ms, respectively, see the Supporting Information). Figure 4a shows that a more adhesive and soft contact is characterized by an efficient triboelectrification occurring since the early times of contact between the two tribomaterials. Upon reaching the maximum force load and during the following force release, a fast detachment is observed for the nonadhesive surfaces (PVA:Li and Al), while the a-PVA:Li film keeps charging for other ≈10 ms before detachment. This is a consequence of the sticky adhesion which maintains the two surfaces in contact for longer time upon gradual release of the external force load. During this time interval an increase in the energy dissipation area occurs, leading to an increased electrification as depicted in the scheme reported in Figure 4b. In the Supporting Information, we report an example of TENGs where a nonadhesive contact is established between the PVA:Li (or the a-PVA:Li) and a Kapton film. In PE the presence of ester functional groups can favor the formation of weak bonds, such as hydrogen bonds, with the a-PVA:Li films which is rich in hydroxyl groups. Compared to PE,

© 2024 The Author(s). Advanced Materials published by Wiley-VCH GmbH

15214095, 2024, 27, Downloaded from https://advanced.onlinelibrary.wiley.com/doi/10.1002/adma.202403366 by Yonsei University Library, Wiley Online Library on [21/08/2025]. See the Terms and Conditions (https://onlinelibrary.wiley.com/terms-and-conditions) on Wiley Online Library for rules of use; OA articles are governed by the applicable Creative Commons License

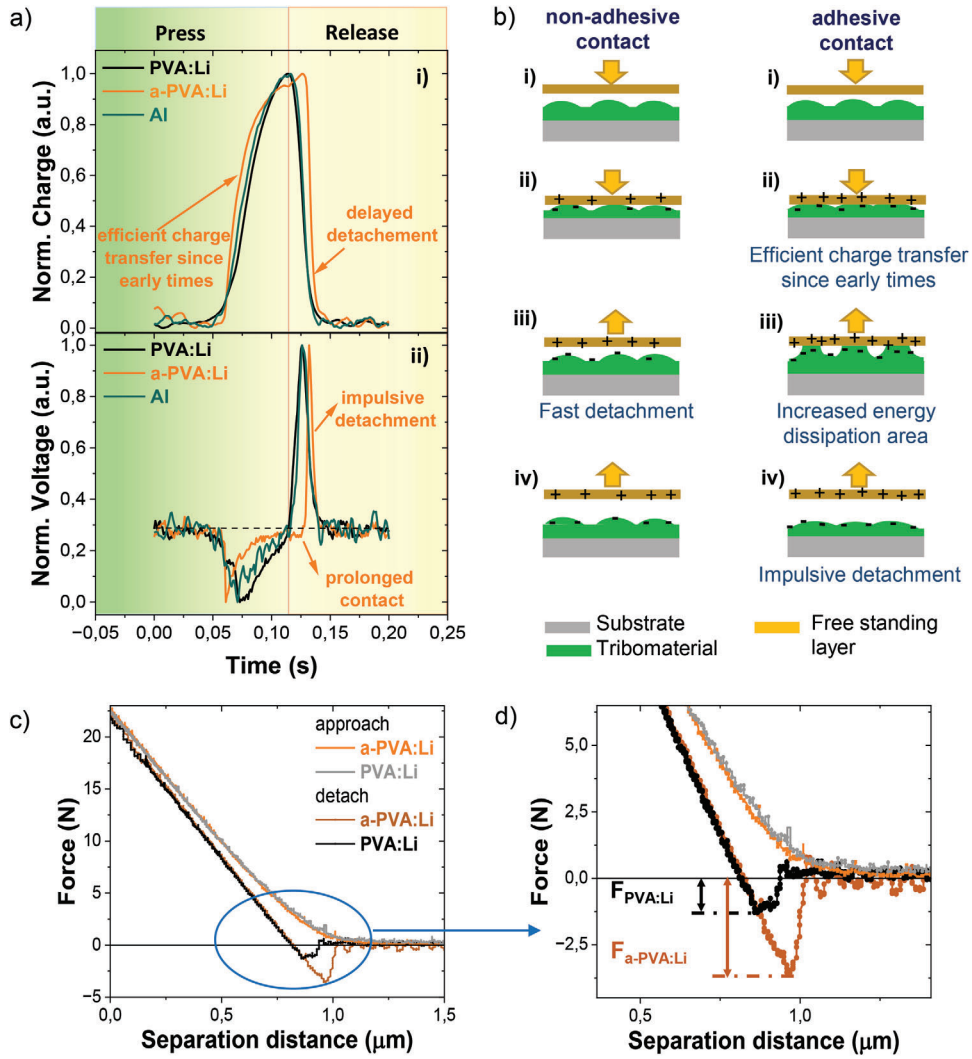

Figure 4. a) Normalized charge (i) and normalized voltage (ii) recorded during a single contact-separation cycle (15 N, 5 Hz). b) Schematic representation of a nonadhesive contact (PVA:Li) and an adhesive contact (a-PVA:Li). c,d) In situ (on devices) force–distance curves acquired during the approach-contact-and-detachment of the a-PVA:Li and PVA:Li films with the reference PE film in their respective TENGs (1-year old samples). $F_{PVA:Li}$ and $F_{a\text{-}PVA:Li}$ refer to the adhesion force measured during contact between the PVA:Li or the a-PVA:Li films with the PE film, respectively.

Kapton is characterized by a more hydrophobic surface that is less prone to such weak interfacial bonding. Therefore, no significant difference could be observed in the voltage dynamics and in the in situ force–distance curves, recorded for the a-PVA:Li and PVA:Li TENGs that incorporated Kapton as reference materials. This further demonstrates the dependence of adhesive forces on the chemical, morphological, and rheological properties of the selected pair of tribomaterials. This experimental evidence also shows that the comparison of the voltage dynamics can be a useful tool to identify the presence of adhesive contact in TENGs. Overall, a more adhesive contact results in i) an efficient charge transfer since the early time of contact, ii) a prolonged adhesion that leads to an increased dissipation energy area and a continued charge transfer even upon force release, and iii) a delayed and more impulsive detachment of the two surfaces (discharge occurring within a shorter time). It is interesting to notice how the efficient triboelectrification occurring since early times, and highlighted in the contact-separation dynamics of the a-PVA:Li based TENGs, is also consistent with the force–distance curves acquired with the AFM probe, where adhesions interactions start to be sensed by the tip at longer distances between the tip and the surface in PVA:Li films (Supporting Information). Another experimental evidence of the more adhesive contact achieved by the a-PVA:Li films is provided by its stronger frequency dependence compared to the PVA:Li (Figure 3c,d). This is consistent with previous reports where at higher frequencies the faster detachment of the adhesive interfaces determines an increase in the dissipation area which is then responsible for an increased triboelectrification charge density.[19]

Overall, the abundance of water molecules, the more amorphous structure and the improved adhesion are factors that synergistically contribute to the improved performance observed in TENGs based on adhesive and ionic a-PVA hydrogel-based films. The water abundance and the amorphous structure can enable

© 2024 The Author(s). Advanced Materials published by Wiley-VCH GmbH

15214095, 2024, 27, Downloaded from https://advanced.onlinelibrary.wiley.com/doi/10.1002/adma.202403366 by Yonsei University Library, Wiley Online Library on [21/08/2025]. See the Terms and Conditions (https://onlinelibrary.wiley.com/terms-and-conditions) on Wiley Online Library for rules of use; OA articles are governed by the applicable Creative Commons License

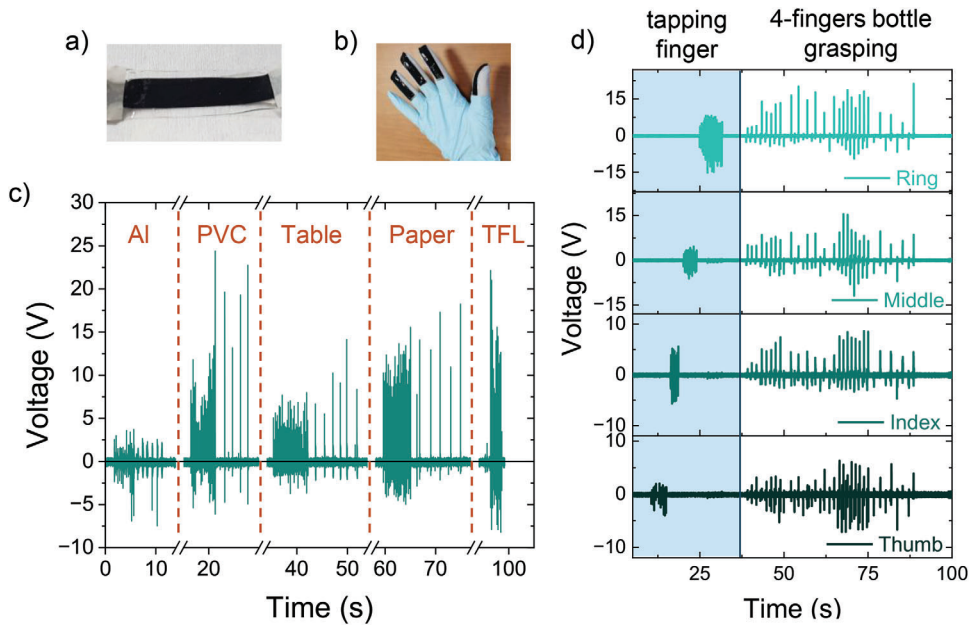

Figure 5. E-skin prototype based on a-PVA:Li films (w/w, 100:20). a,b) Optical photographs of the single electrode TENG used as e-skin. C) Voltage output measured during index finger tapping on different substrates (Al, aluminum; PVC, polyvinyl chloride; resin table; paper; PTFE, polytetrafluoroethylene). D) Voltage output recorded from the sensors applied on each finger as shown in (b), during single finger tapping (up to 40 s) and following synchronous 4-fingers recording acquired during the grasping of a plastic bottle (video in the Supporting Information).

an improved triboelectric charges distribution over the material surface, reducing their electrostatic repulsion, thus leading to the higher charge density observed in a-PVA:Li than in the PVA:Li. Additionally, the improved adhesion observed in the a-PVA:Li compared to the PVA:Li, contribute to a different contact-and-separation dynamics during the TENG operation. Upon adhesive detachment the surface area of the adhesive material increases contributing to harvest more triboelectric charges during the TENGs operation (scheme Figure 4b-iii). As previously reported, the presence of stronger adhesive forces causes a temporal increase in the energy dissipation area during an adhesive detachment,[70] that favors the transfer of more triboelectrification charges. Finally, an important role is also played by the more impulsive detachment which characterizes the mechanics of adhesive contacts. A more impulsive detachment during the release-event causes a faster discharge of the induction charges accumulated at the electrodes during the press-event. This faster charge flow generates more intense current and voltage peaks. Additionally, adhesion in viscoelastic polymers is known to be strongly dependent on the applied load,[71] and on the contact-and-separation rate dynamics[72] thus providing a higher sensitivity to pressure loads and mechanical frequency compared to non-adhesive contacts. The ensemble of the above properties, make the a-PVA:Li hydrogel film a more efficient tribomaterial than PVA:Li, for the development of pressure and tactile sensors.

To demonstrate its application in an e-skin prototype, the conductive a-PVA:Li film was deposited on a carbon-tape used as flexible electrode to form a single electrode TENG (optical images in **Figure** 5a). An e-skin prototype was attached to each of the four hand-fingers as shown in Figure 5b, compatibly with the maximum number of channels available on the oscilloscope. The TENG is than operated in the single electrode mode. Figure 5c shows the voltage output recorded upon finger tapping on different materials, demonstrating the e-skin sensitivity to the chemical composition of the material under contact. Figure 5d shows the synchronous recording of the voltage output generated by each e-skin prototype during the grasping of a plastic bottle (Video in the Supporting Information). Signal intensity and time variation are directly correlated with the touch frequency and the force applied by each finger on the bottle during the grasping events.

2.3. PVA:Li and a-PVA:Li Conductive Hydrogels as Ionic Conductor in Single Layer TENGs

So far, we demonstrated the impact on TENGs performance, of the high water content present in the a-PVA:Li film when employed as tribomaterial. In this section, we show the positive effect of the high and stable water uptake, also when the a-PVA:Li hydrogel is integrated as ionic conductor in single layer TENGs. In this device configuration the ion conductive hydrogel is embedded into an elastomeric shell made of a Si-rubber scaffold which acts both as an encapsulating material and a tribomaterial. A carbon tape (C)-electrode was selected due to its higher stability to alkaline metal corrosion than metal-electrodes. Ungrounded Al foil (free standing floating electrode) was employed as reference material (**Figure** 6-f-g-h). This encapsulation strategy allows to avoid the hydrogel dehydration and to prolong its shelf-life stability (more than 3 months). The best compromise between high ionic concentration and reproducible device assembly process was found for an a-PVA (or PVA):Li ratio of 50:50 w/w. This formulation allows the formation of dense jelly layers that do not fully dry even after 1 week from preparation and upon storage

© 2024 The Author(s). Advanced Materials published by Wiley-VCH GmbH

15214095, 2024, 27, Downloaded from https://advanced.onlinelibrary.wiley.com/doi/10.1002/adma.202403366 by Yonsei University Library, Wiley Online Library on [21/08/2025]. See the Terms and Conditions (https://onlinelibrary.wiley.com/terms-and-conditions) on Wiley Online Library for rules of use; OA articles are governed by the applicable Creative Commons License

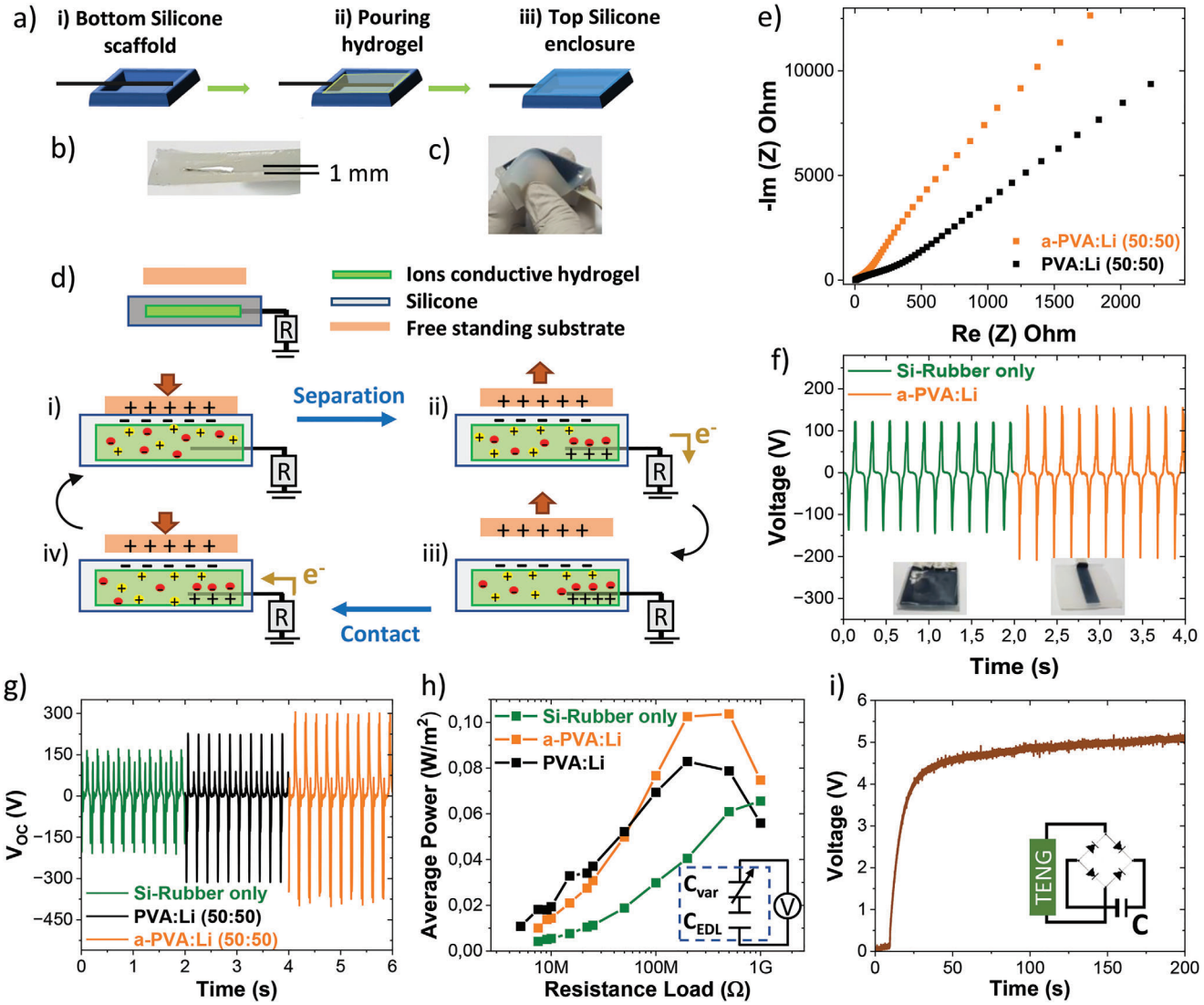

Figure 6. a) Schematic of the procedure employed to fabricate single electrode TENGs based on ion conductive hydrogels (Si-rubber scaffold as active tribomaterial). Optical images showing b) the cross section of the single layer TENG and c) its flexibility. d) Simplified picture of the working mechanism of a TENG incorporating an ionic hydrogel. e) Impedance spectra acquired on PVA:Li and a-PVA:Li (50:50, w/w). f) Voltage output showing improved performance attained with a-PVA:Li ionic electrode compared to C-electrode (40 MΩ voltage probe). Inset optical photograph of the a-PVA:Li and C-electrode based devices. g) Open circuit voltage (V_{OC}). h) Average power comparing a-PVA:Li and PVA:Li single electrode TENGs and Si-rubber only TENG (@5 Hz, 1 cm airgap, 15 N) and inset scheme of the equivalent circuit including the EDL capacitance (C_{EDL}). i) Capacitor charging with a-PVA:Li single electrode TENG (1 µF, 5 V) and simplified scheme of the conditioning circuit (inset).

in ambient condition (≈40% humidity). Furthermore, the quasi-solid state facilitates the easy and reproducible integration of the a-PVA:Li hydrogel into the Si-rubber scaffold, following a layer-by-layer fabrication processing (Figure 6a). Impedance spectra reported in Figure 6e (and in the Supporting Information), confirm the higher EDLC attained with the a-PVA:Li compared to the PVA:Li (50:50 w/w; 50 and 30 mF cm^{-2} respectively). Furthermore, the ionic conductivity in a-PVA:Li increases almost 4-times compared to the PVA:Li (7.4×10^{-4} and 2.0×10^{-4} S cm^{-1} respectively, at room temperature), reaching a value in line with the current state-of-art for best optimized solid-polymer-electrolytes based on Li-salts.[73–75]

A picture of the single electrode TENG showing its flexibility is available in Figure 6c, while in Figure 6b a cross section view of the internal uniform structure of the Si-rubber/hydrogel enclosure is shown (hydrogel layer ≈1 mm thick). The schematic view of the encapsulated hydrogel based TENG and its single electrode mode working mechanism can be found in Figure 6d. The ionic charges responsible for the formation of the EDLC at the C-electrode are also depicted in the schematic. The formation of the EDL layer at the interface with the C-electrode is at the basis of the working mechanism for such single electrode and hydrogel-based TENGs (equivalent circuit scheme in Figure 6h inset).

© 2024 The Author(s). Advanced Materials published by Wiley-VCH GmbH

15214095, 2024, 27, Downloaded from https://advanced.onlinelibrary.wiley.com/doi/10.1002/adma.202403366 by Yonsei University Library, Wiley Online Library on [21/08/2025]. See the Terms and Conditions (https://onlinelibrary.wiley.com/terms-and-conditions) on Wiley Online Library for rules of use; OA articles are governed by the applicable Creative Commons License

During operation, the free-standing material is brought into contact with the single electrode TENG, and triboelectric charge transfer occurs. The density of the triboelectrification charges is dependent on the relative position of the free-standing material and the Si-rubber along the triboelectric series.[76] When in contact with an Al layer, negative triboelectric charges accumulate on the Si-rubber surface. Upon separation, the electrostatic field generated by the negative charges on the silicon surface will promote the migration of the positive ions (Li^+) toward the interface with the silicone, while the negative ions (Cl^-) migrate in the opposite direction and toward the C-electrode. The negative ions migration to the C-electrode recall positive electronic charges from the ground, a process that is responsible for the increase in TENG electrode capacitance due to the formation of the EDL. Reapproaching of the materials will drive ions migration in the opposite direction, and an electronic current will flow back accordingly. The single electrode TENG can then be exploited as an electrical power generator or as a sensor.

Figure 6g,h reports, respectively, the open circuit voltage (V_{OC}) and average power output, measured on single layer TENGs containing no-hydrogel, PVA:Li or a-PVA:Li hydrogels (50:50, w/w). A neat improvement (≈40% increase in average power) is obtained when the a-PVA:Li hydrogel is employed as ionic conductor compared to TENGs containing only the Si-Rubber scaffold (65 mW m^{-2}). A 25% increase in power output is observed for TENGs based on the a-PVA:Li ionic conductors (102 mW m^{-2}) with respect to the one embedding the PVA:Li hydrogel (83 mW m^{-2}). We also observe that for the hydrogel based TENGs, the average power maximum (Figure 6h) is shifted toward lower values of the resistance loads compared to the one containing only the Si-rubber. This is associated to the lower internal impedance of the TENGs based on the ion conducting hydrogels.

TENGs based on the a-PVA:Li conductive hydrogel have also been compared with TENGs where the C-electrode was inserted under the entire active area (Figure 6f). The higher voltage output achieved by the TENG based on the a-PVA:Li conductive hydrogel demonstrates its superior performance with respect to C-electrode, due to the EDL formation. Thus, a significant enhancement of the output power and a reduction of the TENG impedance is possible through increasing the hydrogel conductivity and therefore by raising the EDLC in TENGs. The charging to 5 V of a 1 μF capacitor connected to the single layer TENG is shown in Figure 6i (with Al layer at ground). The single electrode TENGs electrical output is stable and reproducible under continuous operation and can sustain more than 5000 mechanical cycles. Performances are maintained also after keeping the single electrode TENGs under ambient condition for more than 3 months from fabrication.

3. Conclusions

We show that the introduction of ramified hydroxylated side chains in a PVA derivative, can promote a high and stable water uptake in polymer-based hydrogels that leads to more efficient triboelectric generators and sensors. Such improvement is favored by the synergistic effect of the amorphous morphology and strong water entrapment into the polymer 3D-network, which consequently allows for higher ionic mobility, increased material softness, surface adhesion, and flexibility compared to the PVA homopolymer. In the a-PVA:Li presented in the current work, most of the water species entrapped in the polymer matrix can be removed only at temperatures significantly higher than those characteristics of free and bound water.

When used as tribomaterial in single layer TENGs, the a-PVA shows higher force sensitivity with respect to the homopolymer, and its effective use as e-skin for tactile sensing has been demonstrated. It is highlighted that the observed high sensitivity and large linearity range could be obtained with single layer, non-fluorinated, and nonpatterned tribomaterial, and only by an improved polymer chemical composition. We also provide a detailed description of the adhesive contact mechanism that is behind the observed high-pressure sensitivity. Specifically, the higher and more stable water uptake characterizing the a-PVA:Li films compared to the PVA:Li, is responsible for the increased surface adhesion, thus for an increase in energy dissipation area and contact electrification during TENG operation in contact/separation mode. Overall, we identified different factors that synergistically contribute to increase the pressure sensitivity of TENGs based on adhesive and ionic hydrogel-based films, that are i) the reduced electrostatic repulsions among the surface triboelectric charges favored by the presence of ions and strongly absorbed water; ii) the increased energy dissipation area occurring during detachment that temporally increase the triboelectric surface area iii) the adhesive contact that originates an impulsive detachment which is strongly dependent on force and mechanical rate dynamic.

The a-PVA based TENGs shows excellent stability both over time (up to 1 year from deposition) and under continuous contact-separation cycling (more than 5000 cycles). The favorable impact of the higher and more stable water uptake achieved in the a-PVA ionic hydrogels is also demonstrated with TENGs operating in single electrode mode that integrate the hydrogel as an ionic conductor. A more efficient formation of the EDL at the interface between the hydrogel and the electrode, fostered by the higher ionic mobility found in a-PVA:Li with respect to PVA:Li, is shown to be responsible for the improved electrical output. Considering the high transparency and biocompatibility of PVA, carefully engineered PVA derivatives hold large potential prospects in biomedical applications as in e-skin, health monitoring, and implantable electronics.

4. Experimental Section

Hydrogel Formulation: Poly(vinyl alcohol) (PVA, from Merk, > 99% hydrolyzed, M_w = 146 000–186 000), the PVA copolymer (a-PVA, from Nighigo G-Polymer, OKS 1089, polymerization degree 2500 data from supplier, approximate M_w = 300 000) and the LiCl (from Merk) were used without any further purification. The safety and nongenotoxicity of the G-Polymer employed in this work was certified from the European Food Safety Authority.[77–79]

The hydrogel was prepared by pouring the PVA (or a-PVA) powder in deionized water under vigorous magnetic stirring to reach a concentration of 100 g L^{-1}. To obtain the complete dissolution of the polymer particulates in PVA solutions it is necessary to raise the heating temperature up to 135–140 °C for at least ≈10–15 min. For the a-PVA clear solution are obtained already at 100 °C (≈10–15 min). Each solution was then kept under vigorous stirring at 80 °C for at least 1 h. The 100 mg mL^{-1} a-PVA can also be prepared at 80 °C and under continuous stirring (≈3 h) with no preheating. Such lower temperature processing does not allow to fully dissolve high molecular weight PVA as the one used in the current work.

© 2024 The Author(s). Advanced Materials published by Wiley-VCH GmbH

15214095, 2024, 27, Downloaded from https://advanced.onlinelibrary.wiley.com/doi/10.1002/adma.202403366 by Yonsei University Library, Wiley Online Library on [21/08/2025]. See the Terms and Conditions (https://onlinelibrary.wiley.com/terms-and-conditions) on Wiley Online Library for rules of use; OA articles are governed by the applicable Creative Commons License

Conducting hydrogels employed as triboelectric materials are obtained by dissolving 100 g L^{-1} of the polymer (PVA or a-PVA) with a 50 g L^{-1} LiCl salt in water solution (100:20, w/w ratio). This weight ratio allows to obtain films that can dry overnight.

Conducting hydrogels employed as electrolytic electrode are obtained by dissolving 50 g L^{-1} of the polymer (PVA or a-PVA) with a 50 g L^{-1} LiCl salt in water solution (50:50, w/w ratio). These conductive hydrogels slowly lose their water and remain wet for more than a week (in the case of a-PVA conductive hydrogel more than 2 weeks).

Thermal and mechanical analysis were performed on hydrogels films deposited on a PTFE substrate 1 mL of the hydrogel (100:20 w/w solutions) were deposited over a 4.5 × 4.5 cm^2 PTFE substrates, dried overnight under controlled atmosphere (21 °C and 40% humidity) and measured within 1 week from deposition. The use of PTFE substates allow to peel-off the dried films, making it available as free-standing film for the following spectroscopic, thermal, and mechanical measurements.

Confocal Micro-Raman Spectroscopy: Raman spectra are acquired using a Renishaw In-Via spectrometer (New Mills, Kingswood, Wotton-under-Edge, UK) equipped with a solid-state laser source and excitation wavelength of 514 nm (2.41 eV). The laser power was set below 10% of its nominal power (< 1 mW) to avoid sample damage.

Thermal Characterization: Differential scanning calorimeter was performed with a DSC-Q1000 from TA in a flowing N_2 atmosphere with a gas flow rate of 50 mL min^{-1}. The DSC curves of samples were recorded at scanning rate of 10 °C min^{-1} during first heating of the as-prepared samples from 25 to 250 °C, cooling from the melt to 25 °C and successive heating from 25 to 250 °C.

A rough estimation of the samples crystallinity degree (X_c) was calculated from the following equation as previously reported:[80–82]

$$X_C = \frac{\Delta H_m * 100}{\Delta H_m^\circ} \quad (1)$$

where ΔH_m is the melting temperature value of the sample determined from the I-heating and ΔH_m° is the reference melting enthalpy value of 156 J g^{-1} for 100% crystalline PVA.

Thermo-gravimetric analysis (TGA) was carried out in N_2 flow (flow rate = 40 mL min^{-1}) using a TGAQ500-TA Instruments, at heating rate of 10 °C min^{-1} in the temperature range from 25 to 350 °C.

TGA data of each hydrogel film were validated by triplicate measurements.

The free-water contained in each hydrogel film was extracted from the weight loss detected at 100 °C, which is associated to the free-water molecules evaporation. The weight losses occurring at higher temperatures are than associated to water molecules that interact with the polymer chain or the ions (Li^+, Cl^-) with stronger interactions than the H-bonds holding water molecules in the liquid phase.[83]

Nanoindentation Characterization: Nanoindentation tests were performed using Micro Materials Ltd.'s NanoTest Platform III with a Berkovich indenter.

Samples were cut into small 60 mm × 60 mm squares and glued with a cyanoacrylate adhesive onto an aluminum stub. The samples were left in the test chamber for 3 h before testing began. This time was necessary to stabilize the temperatures of the indenter and sample at the same value of 36 °C, to minimize thermal drift. The mechanical tests were performed by controlling the maximum depth penetration, which was set at 500 nm to avoid interference from the underlying metal substrate. This depth was achieved with the indenter penetration set at a loading rate of 0.05 mN s^{-1}. During indentation, the device recorded the load and the indenter displacement (penetration inside the material starting from zero level at the surface). Once the maximum penetration depth was reached, to avoid residual viscoelastic effects, a holding time of 60 s was set before the unloading ramp at the set loading rate. To check the repeatability of the values of the individual indentations and the homogeneity of the samples, 20 indentation tests were performed over different areas per each sample (i.e., loading up to 500 nm, holding the maximum reached load for 60 s and unloading at 0.05 mN s^{-1}), and by selecting the indentation position at 50 µm from each other to exclude interaction effects.

From each loading–unloading curve, the hardness, H, and reduced elastic modulus, E_r, of the coatings were calculated according to the following Equations (2) and (3), respectively:

$$H = \frac{L_{MAX}}{A_C} \quad (2)$$

$$Er = \frac{\sqrt{\pi} S_{MAX}}{2\sqrt{A_c}} \quad (3)$$

where L_{MAX} is the maximum indentation load, A_c is the projected contact area, which for a perfectly sharp Berkovich indenter is calculated as $A_c = 24.56 h_c^2$ with h_c equal to contact depth and S_{MAX} is the slope of unloading curve at the maximum load.[84–86]

In Situ (On-Device) Force–Distance Curves: For this measurement a home-made electromechanical setup was employed. The two triboelectrodes (triboelectric material coated electrode) constituting the TENG device are brought into contact and detached at a speed of 1 mm s^{-1}. The maximum applied force (20 N) is held for 5 min before full detachment of the two triboelectrodes (final separation 1 cm). The on-device force–distance curves have been acquired on 1 year old samples.

Atomic Force Microscopy and Force–Distance Curves: Atomic force microscopy (AFM) images and force–distance curves were acquired with a Dimension Icon, Bruker, USA. Adhesion force measurements were acquired using Nanosensors Si-tips (PPP-NCH-20, Force constant 49 N m^{-1}) and are acquired by sampling the surface area in 10 different points and by recording at least 25 force–distance curves per each point. Samples more than 8-months old were employed to validate the persistent softness and adhesion properties of the a-PVA:Li sample over time. Force-distance curves acquired on pristine films (PVA and a-PVA) are reported in the Supporting Information. The relation between the pull-off force and the work of adhesion is given in the Supporting Information.

Impedance Spectroscopy: Impedance spectroscopy was performed with an impedance analyzer (E4980AL-032, Keysight). Spectra were acquired 0 V direct voltage (V_{DC}) and 10 mV alternate voltage (V_{AC}) amplitude was used to study the capacitive and resistive properties of the hydrogel films. The electrochemical characterization of the electrolyte gel composites was performed in a Swagelok cell in symmetric electrolytic capacitor configuration and Al electrodes (electrolytic capacitor area 0.196 cm^2). The polymeric films were deposited on an Al substrate before measurement. Films were measured the day after the hydrogel deposition.

TENG Fabrication: Three different device configurations have been developed where the hydrogel layer was employed either as the active triboelectric materials in TENGs operated in contact-separation mode or as single-layer e-skin, or as electrolytic electrode in encapsulated into and elastomeric triboelectric material (Si-rubber, Si-TENGs).

For hydrogels TENGs operated in contact-separation mode (generator and sensors) and as e-skin the hydrogels were cast onto either an Al foil or C-tape employed as electrodes. Pre-charged polytetrafluoroethylene (PTFE) was obtained by rubbing the PTFE surface with gloves. In comparative studies, the second triboelectrode was composed of a polyester tape (70 µm thick from MERK) sticked on Al electrodes (50 µm). 1 mL of the hydrogel (100 g L^{-1} or 100:20 conductive solution) was cast over an electrode area of 4.5 × 4.5 cm^2. The gel composites were left drying in a controlled atmosphere (humidity 40%, temperature 20–21 °C) overnight before integration into the TENGs. Upon drying the hydrogel thickness was 50 µm.

For the preparation of the Si-TENGs the 50:50 w/w (polymer/LiCl) hydrogel formulation was employed. The Si-rubber was prepared by mixing two components the resins and hardener as provided by the supplier. The bottom layer (1.5 mm thick) was prepared by pouring the Si-Rubber composite into an acrylic mold and left solidifying at room temperature overnight. Then a C-tape stripe (0.8 cm × 4 cm) was attached to one side of the silicone mold before the conductive hydrogel was poured in it. The conductive hydrogel was let to partially dry overnight (1 mm thick). This

© 2024 The Author(s). Advanced Materials published by Wiley-VCH GmbH

15214095, 2024, 27, Downloaded from https://advanced.onlinelibrary.wiley.com/doi/10.1002/adma.202403366 by Yonsei University Library, Wiley Online Library on [21/08/2025]. See the Terms and Conditions (https://onlinelibrary.wiley.com/terms-and-conditions) on Wiley Online Library for rules of use; OA articles are governed by the applicable Creative Commons License

drying step allows the formation of a uniform 100 µm thick conducting hydrogel layer that can sustain the following step consisting in the deposition of a second layer of Si-rubber composite. The second Si-rubber layer (1.5 mm thick) was playing the function of both triboelectric material and encapsulating film.

TENG Characterization: TENG output was measured with a home-built set-up comprising a linear motor, a load cell, an oscilloscope (Tektronix MSO5000), a voltage probe 40 MΩ (Tektronix), a current amplifier (1211 DL Instruments), and a home-built resistance commutator for current measurements. The open circuit voltage (V_{OC}) was measured using a 1 GΩ voltage probe (1000x Tektronix), that is almost 2 orders of magnitude higher than the impedance value found at power maximum (50 MΩ). This ensures that are under experimental zero current condition, thus providing an accurate measurement of the V_{OC}.

The device active area was 4×4 cm^2. The maximum air gap between the two triboelectrodes was set at 5 mm. The instant peak power was calculated from the current peak maximum measured at varying resistance loads ($P_{ave} = R_{Load} \times {I_{Peak}}^2$). The average power was calculated according to the formula:[87]

$$P_{ave} = \frac{1}{T} \int_0^T I^2 R dt \tag{4}$$

with T being the time interval of an entire cycle at 5 Hz.

A commercial LTC-3588 energy harvester or a rectifier bridge (ST BAT 47 diodes bridge) coupled with an electrolytic capacitor (1 µF, 5 V) were used to demonstrate the capability of the TENGs to charge a storage unit. The Al layer was grounded according to the LTC3588 required connections.

The sensitivity reported in the main text is calculated according to the following equation:

$$S = \frac{\Delta V}{\Delta P} \tag{5}$$

Were ΔV is the voltage difference between the maximum and minimum measured voltage and ΔP is the difference between the maximum and minimum pressure applied. The sensitivity calculated according to Equation (5) is 2.1 V kPa^{-1} for a-PVA:Li; 0.9 V kPa^{-1} for PVA:Li Li, detected at 5 Hz in the applied pressure range of from 1 to 14 kPa (or also 1.3 N V^{-1} for a-PVA:Li; 0.5 V N^{-1} for PVA:Li Li; 16 cm^2 active area).

For the e-skin testing and during the hand grasping of a plastic bottle demonstration, a 10 MΩ probe was connected to each of the 4-fingers sensor for the synchronous recording on the oscilloscope.

Supporting Information

Supporting Information is available from the Wiley Online Library or from the author.

Acknowledgements

The authors knowledged Dr. Stefano Brivio for video acquisition and Mario De Angioletti (IPCB-CNR) for the nanoindentation analysis. The authors would like to acknowledge the support provided by the PNRR project titled Infrastructure for Energy Transition and Circular Economy @ Euro-NanoLab – iENTRANCE@ENL, funded by MUR No. 0000128.

Conflict of Interest

The authors declare no conflict of interest.

Data Availability Statement

The data that support the findings of this study are available from the corresponding author upon reasonable request.

Keywords

contact adhesion, electrochemical capacitance, e-skin, solid-state electrolytes, supercapacitors, TENG sensors

Received: March 5, 2024
Revised: April 11, 2024
Published online: April 30, 2024

[1] Z. L. Wang, *Mater. Today* **2017**, *20*, 74.
[2] Y. Zi, H. Guo, Z. Wen, M. H. Yeh, C. Hu, Z. L. Wang, *ACS Nano* **2016**, *10*, 4797.
[3] J. Zhao, G. Zhen, G. Liu, T. Bu, W. Liu, X. Fu, P. Zhang, C. Zhang, Z. L. Wang, *Nano Energy* **2019**, *61*, 111.
[4] Q. Zhang, C. Xin, F. Shen, Y. Gong, Y. L. Zi, H. Guo, Z. Li, Y. Peng, Q. Zhang, Z. L. Wang, *Energy Environ. Sci.* **2022**, *15*, 3688.
[5] Q. Zhang, Z. Zhang, Q. Liang, F. Gao, F. Yi, M. Ma, Q. Liao, Z. Kang, Y. Zhang, *Nano Energy* **2019**, *55*, 151.
[6] M. Haghayegh, R. Cao, F. Zabihi, R. Bagherzadeh, S. Yang, M. Zhu, *J. Mater. Chem. C* **2022**, *10*, 11439.
[7] W. Xu, M. C. Wong, J. Hao, *Nano Energy* **2019**, *55*, 203.
[8] M. H. Lee, W. Wu, *Adv. Mater. Technol.* **2022**, *7*, 2101623.
[9] Q. Duan, W. Peng, J. He, Z. Zhang, Z. Wu, Y. Zhang, S. Wang, S. Nie, *Small Methods* **2023**, *7*, 2201251.
[10] B. Jiang, Y. Long, X. Pu, W. Hu, Z. L. Wang, *Nano Energy* **2021**, *86*, 106086.
[11] X. Xie, X. Chen, C. Zhao, Y. Liu, X. Sun, C. Zhao, Z. Wen, *Nano Energy* **2021**, *79*, 105439.
[12] G. Pace, A. E. del Rio Castillo, A. Lamperti, S. Lauciello, F. Bonaccorso, *Adv. Mater.* **2023**, *35*, 2211037.
[13] L. Jin, X. Xiao, W. Deng, A. Nashalian, D. He, V. Raveendran, C. Yan, H. Su, X. Chu, T. Yang, W. Li, W. Yang, J. Chen, *Nano Lett.* **2020**, *20*, 6404.
[14] Z. Peng, X. Xiao, J. Song, A. Libanori, C. Lee, K. Chen, Y. Gao, Y. Fang, J. Wang, Z. Wang, J. Chen, M. K. H. Leung, *ACS Nano* **2022**, *16*, 20251.
[15] L. Shi, S. Dong, H. Xu, S. Huang, Q. Ye, S. Liu, T. Wu, J. Chen, S. Zhang, S. Li, X. Wang, H. Jin, J. M. Kim, J. Luo, *Nano Energy* **2019**, *64*, 103960.
[16] H. Ryu, J. H. Lee, T. Y. Kim, U. Khan, J. H. Lee, S. S. Kwak, H. J. Yoon, S. W. Kim, *Adv. Energy Mater.* **2017**, *7*, 1700289.
[17] G. Pace, A. Ansaldo, M. Serri, S. Lauciello, F. Bonaccorso, *Nano Energy* **2020**, *76*, 104989.
[18] G. Pace, M. Serri, A. E. del R. Castillo, A. Ansaldo, S. Lauciello, M. Prato, L. Pasquale, J. Luxa, V. Mazánek, Z. Sofer, F. Bonaccorso, *Nano Energy* **2021**, *87*, 106173.
[19] L. Zhang, Y. Zhang, X. Li, Y. Feng, B. Yu, F. Zhou, D. Wang, *Nano Energy* **2022**, *95*, 107011.
[20] K. Shi, B. Chai, H. Zou, Z. Wen, M. He, J. Chen, P. Jiang, X. Huang, *Adv. Funct. Mater.* **2023**, *33*, 2307678.
[21] D. Kim, I. W. Tcho, I. K. Jin, S. J. Park, S. B. Jeon, W. G. Kim, H. S. Cho, H. S. Lee, S. C. Jeoung, Y. K. Choi, *Nano Energy* **2017**, *35*, 379.
[22] L. Zhang, Y. Zhang, X. Li, Y. Feng, B. Yu, F. Zhou, D. Wang, *Nano Energy* **2022**, *95*, 107011.
[23] H. Zhang, S. Feng, D. He, Y. Xu, M. Yang, J. Bai, *Nano Energy* **2018**, *48*, 256.
[24] C. W. Peak, J. J. Wilker, G. Schmidt, *Colloid Polym. Sci.* **2013**, *291*, 2031.
[25] M. Ciavarella, J. Joe, A. Papangelo, J. R. Barber, *J. R. Soc. Interface* **2019**, *16*, 20180738.
[26] C. Yang, Z. Suo, *Nat. Rev. Mater.* **2018**, *3*, 125.
[27] T. Zhu, Y. Ni, G. M. Biesold, Y. Cheng, M. Ge, H. Li, J. Huang, Z. Lin, Y. Lai, *Chem. Soc. Rev.* **2022**, *52*, 473.
[28] J. Liu, S. Qu, Z. Suo, W. Yang, *Natl. Sci. Rev.* **2021**, *8*, nwaa254.

© 2024 The Author(s). Advanced Materials published by Wiley-VCH GmbH

15214095, 2024, 27, Downloaded from https://advanced.onlinelibrary.wiley.com/doi/10.1002/adma.202403366 by Yonsei University Library, Wiley Online Library on [21/08/2025]. See the Terms and Conditions (https://onlinelibrary.wiley.com/terms-and-conditions) on Wiley Online Library for rules of use; OA articles are governed by the applicable Creative Commons License

[29] H. Yang, F. R. Fan, Y. Xi, W. Wu, *Adv. Sustainable Syst.* **2020**, *4*, 2000108.
[30] J. Sun, H. Choi, S. Cha, D. Ahn, M. Choi, S. Park, Y. Cho, J. Lee, T. eon Park, J. J. Park, *Adv. Funct. Mater.* **2022**, *32*, 2109139.
[31] Z. Jin, F. Zhao, Y. Lei, Y. C. Wang, *Nano Energy* **2022**, *95*, 106988.
[32] N. A. Mini-review, S. Wang, X. Jing, H. Mi, Z. Chen, J. Zou, Z. Liu, P. Feng, *Polymers* **2022**, *14*, 1452.
[33] L. Zhang, S. Wang, Z. Wang, Z. Huang, P. Sun, F. Dong, H. Liu, D. Wang, X. Xu, *Mater. Horiz.* **2023**, *10*, 2271.
[34] X. Han, D. Jiang, X. Qu, Y. Bai, Y. Cao, R. Luo, Z. Li, *Sci. Adv.* **2017**, *3*, 1700015.
[35] B. Bagchi, P. Datta, C. S. Fernandez, L. Xu, P. Gupta, W. Huang, A. L. David, D. Siassakos, S. Homer-Vanniasinkam, M. K. Tiwari, *Nano Energy* **2023**, *107*, 108127.
[36] W. Xu, L. B. Huang, M. C. Wong, L. Chen, G. Bai, J. Hao, *Adv. Energy Mater.* **2017**, *7*, 1601529.
[37] S. H. Chou, H. W. Lu, T. C. Liu, Y. T. Chen, Y. L. Fu, Y. H. Shieh, Y. C. Lai, S. Y. Chen, *Adv. Sci.* **2023**, *10*, 2202815.
[38] M. Yang, X. Tian, T. Hua, *ACS Appl. Mater. Interfaces* **2023**, *15*, 11802.
[39] P. Zhang, Y. Chen, Z. H. Guo, W. Guo, X. Pu, Z. L. Wang, *Adv. Funct. Mater.* **2020**, *30*, 1909252.
[40] H. Patnam, S. A. Graham, P. Manchi, M. V. Paranjape, J. S. Yu, *ACS Appl. Mater. Interfaces* **2023**, *15*, 16768.
[41] Y. Liu, T. H. Wong, X. Huang, C. K. Yiu, Y. Gao, L. Zhao, J. Zhou, W. Park, Z. Zhao, K. Yao, H. Li, H. Jia, J. Li, J. Li, Y. Huang, M. Wu, B. Zhang, D. Li, C. Zhang, Z. Wang, X. Yu, *Nano Energy* **2022**, *99*, 107442.
[42] G. Li, J. Zhang, F. Huang, S. Wu, C. H. Wang, S. Peng, *Nano Energy* **2021**, *88*, 106289.
[43] L. Guadagno, M. Raimondo, M. Catauro, A. Sorrentino, E. Calabrese, *J. Therm. Anal. Calorim.* **2022**, *147*, 5463.
[44] M. I. Baker, S. P. Walsh, Z. Schwartz, B. D. Boyan, *J. Biomed. Mater. Res. B: Appl. Biomater.* **2012**, *100 B*, 1451.
[45] N. Ben Halima, *RSC Adv.* **2016**, *6*, 39823.
[46] A. V. Nasalapure, R. K. Chalannavar, D. R. Kasai, K. R. Reddy, A. V. Raghu, *Nano Express* **2021**, *2*, 030003.
[47] N. Alexandre, J. Ribeiro, A. Gärtner, T. Pereira, I. Amorim, J. Fragoso, A. Lopes, J. Fernandes, E. Costa, A. Santos-Silva, M. Rodrigues, J. D. Santos, A. C. Maurício, A. L. Luís, *J. Biomed. Mater. Res. A* **2014**, *102*, 4262.
[48] Q. Liang, Q. Zhang, X. Yan, X. Liao, L. Han, F. Yi, M. Ma, Y. Zhang, *Adv. Mater.* **2017**, *29*, 1604961.
[49] J. Fan, M. Yuan, L. Wang, Q. Xia, H. Zheng, A. Zhou, *Nano Energy* **2023**, *105*, 107973.
[50] X. Luo, L. Zhu, Y. C. Wang, J. Li, J. Nie, Z. L. Wang, *Adv. Funct. Mater.* **2021**, *31*, 2104928.
[51] D. Moreau, C. Chauvet, F. Etienne, F. P. Rannou, L. Corté, *Proc. Natl. Acad. Sci. USA* **2016**, *113*, 13295.
[52] Z. Zhang, S. Guo, K. Wang, Q. Zhang, Q. Fu, *Polymer* **2022**, *243*, 124608.
[53] F. G. Torres, O. P. Troncoso, G. E. De-la-Torre, *Int. J. Energy Res.* **2022**, *46*, 5603.
[54] M. Shibutani, T. Kanda, T. Yamamoto, K. Tokumitsu, *Z. JJ. Soc. Mater. Sci., Jpn.* **2017**, *66*, 23.
[55] N. Yan, F. Capezzuto, G. G. Buonocore, M. Lavorgna, H. Xia, L. Ambrosio, *ACS Appl. Mater. Interfaces* **2015**, *7*, 22678.
[56] X. Xiong, J. Liang, W. Wu, *Nano Energy* **2023**, *113*, 108542.
[57] W. Li, J. Dong, X. Zhang, F. R. Fan, *Adv. Mater. Technol.* **2023**, *8*, 2200834.
[58] H. B. Xu, J. H. Kim, S. Kim, H. J. Hwang, D. Maurya, D. Choi, C. Y. Kang, H. C. Song, *Nano Energy* **2019**, *62*, 144.
[59] Y. C. Lai, J. Deng, R. Liu, Y. C. Hsiao, S. L. Zhang, W. Peng, H. M. Wu, X. Wang, Z. L. Wang, *Adv. Mater.* **2018**, *30*, 1801114.
[60] K. Arai, M. Okuzono, T. Shikata, *Macromolecules* **2015**, *48*, 1573.
[61] P. Russo, V. Speranza, A. Vignali, F. Tescione, G. G. Buonocore, M. Lavorgna, *AIP Conf. Proc.* **2015**, *1695*, 020035.
[62] C. C. Yang, Y. J. Lee, S. J. Chiu, K. T. Lee, W. C. Chien, C. T. Lin, C. A. Huang, *J. Appl. Electrochem.* **2008**, *38*, 1329.
[63] R. Iwamoto, M. Miya, S. Mima, *J. Polym. Sci. Polym. Phys. Ed.* **1979**, *17*, 1507.
[64] A. Martinelli, A. Matic, P. Jacobsson, L. Börjesson, M. A. Navarra, A. Fernicola, S. Panero, B. Scrosati, *Solid State Ion* **2006**, *177*, 2431.
[65] M. P. Rosenwinkel, R. Andersson, J. Mindemark, M. Schönhoff, *J. Phys. Chem. C* **2020**, *124*, 23588.
[66] Z. H. Ping, Q. T. Nguyen, S. M. Chen, J. Q. Zhou, Y. D. Ding, *Polymer* **2001**, *42*, 8461.
[67] Y. Jiang, K. T. Turner, *Extreme Mech. Lett.* **2016**, *9*, 119.
[68] B. Cappella, S. K. Kaliappan, H. Sturm, *Macromolecules* **2005**, *38*, 1874.
[69] D. Sychev, S. Schubotz, Q. A. Besford, A. Fery, G. K. Auernhammer, *J. Colloid Interface Sci.* **2023**, *642*, 216.
[70] L. Zhang, Y. Zhang, X. Li, Y. Feng, B. Yu, F. Zhou, D. Wang, *Nano Energy* **2022**, *95*, 107011.
[71] A. J. Baker, S. B. Vishnubhotla, R. Chen, A. Martini, T. D. B. Jacobs, *Nano Lett.* **2022**, *22*, 5954.
[72] A. Petroli, M. Petroli, M. Romagnoli, M. Geoghegan, *Polymer* **2022**, *262*, 125445.
[73] L. C. Tomé, L. Porcarelli, J. E. Bara, M. Forsyth, D. Mecerreyes, *Mater. Horiz.* **2021**, *8*, 3239.
[74] X. Wang, R. Kerr, F. Chen, N. Goujon, J. M. Pringle, D. Mecerreyes, M. Forsyth, P. C. Howlett, *Adv. Mater.* **2020**, *32*, 1905219.
[75] Y. An, X. Han, Y. Liu, A. Azhar, J. Na, A. K. Nanjundan, S. Wang, J. Yu, Y. Yamauchi, *Small* **2022**, *18*, 2103617.
[76] X. Zhang, L. Chen, Y. Jiang, W. Lim, S. Soh, *Chem. Mater.* **2019**, *31*, 1473.
[77] A. Anadón, D. Bell, M.-L. Binderup, W. Bursch, L. Castle, R. Crebelli, K.-H. Engel, R. Franz, N. Gontard, T. Haertlé, T. Husøy, K.-D. Jany, C. Leclercq, J.-C. Lhuguenot, W. Mennes, M. R. Milana, K. Pfaff, K. Svensson, F. Toldrá, R. Waring, D. Wölfle, *EFSA J.* **2009**, *7*, 1324.
[78] A. Anadón, M.-L. Binderup, W. Bursch, L. Castle, R. Crebelli, K.-H. Engel, R. Franz, N. Gontard, T. Haertlé, T. Husøy, K.-D. Jany, C. Leclercq, J.-C. Lhuguenot, W. Mennes, M. R. Milana, K. Pfaff, K. Svensson, F. Toldrá, R. Waring, D. Wölfle, *EFSA J.* **2011**, *9*, https://doi.org/10.2903/j.efsa.2011.2306.
[79] F. I. P. Unit, A. D. Domenico, P. Tobback, A. M. Rinco, *EFSA J.* **2014**, *12*, https://doi.org/10.2903/j.efsa.2014.3820.
[80] A. S. Asran, K. Razghandi, N. Aggarwal, G. H. Michler, T. Groth, *Biomacromolecules* **2010**, *11*, 3413.
[81] K. Z. Donato, M. Lavorgna, R. K. Donato, M. G. Raucci, G. G. Buonocore, L. Ambrosio, H. S. Schrekker, R. S. Mauler, *ACS Sustainable Chem. Eng.* **2017**, *5*, 1094.
[82] J. I. K. Herman, F. Mark, *Encyclopedia of Polymer Science and Engineering*, Wiley & Sons, New York, **1987**, Vol. *4*.
[83] H. Roozendaal, M. Abu-Hardan, R. A. Frazier, *J. Food Eng.* **2012**, *111*, 606.
[84] I. N. Sneddon, *Int. J. Eng. Sci.* **1965**, *3*, 47.
[85] E. A. Filomena Piscitelli, A. M. Scamardella, V. Romeo, M. Lavorgna, G. Barra, *J. Appl. Polym. Sci.* **2012**, *124*, 616.
[86] M. Krumova, A. Flores, F. J. Baltá Calleja, S. Fakirov, *Colloid. Polym. Sci.* **2002**, *280*, 591.
[87] H. Zhang, Y. Lu, A. Ghaffarinejad, P. Basset, *Nano Energy* **2018**, *51*, 10.

© 2024 The Author(s). Advanced Materials published by Wiley-VCH GmbH

15214095, 2024, 27, Downloaded from https://advanced.onlinelibrary.wiley.com/doi/10.1002/adma.202403366 by Yonsei University Library, Wiley Online Library on [21/08/2025]. See the Terms and Conditions (https://onlinelibrary.wiley.com/terms-and-conditions) on Wiley Online Library for rules of use; OA articles are governed by the applicable Creative Commons License